Smart Materials and Structures

PAPER • OPEN ACCESS

Experimental investigations of the effects of bending vibrations resonance modes on penetration into granular materials

To cite this article: Mahdi Alaei Varnosfaderani *et al* 2024 *Smart Mater. Struct.* **33** 065019

View the article online for updates and enhancements.

You may also like

- A novel traveling wave piezoelectric actuated wheeled robot: design, theoretical analysis, and experimental investigation
Botao Jia, Liang Wang, Ruifeng Wang et al.

- A novel rotary ultrasonic motor based on multiple Langevin transducers: design, simulation, and experimental investigation
Xinchi Ma, Ying Yang, Jianmin Qiu et al.

- A novel structural–functional integration piezoelectric thruster for miniature unmanned underwater vehicles
Rui Liu, Heng Zhao, Liang Wang et al.

This content was downloaded from IP address 132.207.4.76 on 10/06/2024 at 17:46

OPEN ACCESS
IOP Publishing
Smart Materials and Structures
Smart Mater. Struct. **33** (2024) 065019 (18pp)
https://doi.org/10.1088/1361-665X/ad4758

Experimental investigations of the effects of bending vibrations resonance modes on penetration into granular materials

Mahdi Alaei Varnosfaderani[1], **Nan Wu**[4] **and Pooneh Maghoul**[1,2,3,*]

[1] Sustainable Infrastructure and Geoengineering Laboratory (SIGLab), Department of Civil Engineering, Price Faculty of Engineering, University of Manitoba, Winnipeg, Canada
[2] Sustainable Infrastructure and Geoengineering Laboratory (SIGLab), Department of Civil, Geological and Mining Engineering, Polytechnique Montreal, Montreal, Canada
[3] Space Resources and Infrastructure Engineering Research Unit (ASTROLITH), Polytechnique Montreal, Montreal, Canada
[4] Department of Mechanical Engineering, Price Faculty of Engineering, University of Manitoba, Winnipeg, Canada

E-mail: pooneh.maghoul@polymtl.ca, alaeivam@myumanitoba.ca and nan.wu@umanitoba.ca

Received 8 January 2024, revised 5 April 2024
Accepted for publication 3 May 2024
Published 16 May 2024

Abstract

Inspired by the bending vibration observed in the biological locomotions such as those found in snakes, horned lizards, and sandfish, we have developed a novel vibro probe utilizing bending resonance modes to study the bending vibration effects in assisting penetration into granular materials. This approach contrasts with traditional probes that rely on longitudinal vibrations for penetration. This newly developed probe was used to experimentally investigate the impact of bending vibration in reducing the required penetration force and enhancing the penetration process within granular materials such as lunar or Martian regolith. The bending vibrations were excited by thin piezo patches attached to the probe's machined surface without increasing the probe's outside diameter. This simple mechanism enables pushing the whole probe inside the granular materials. Experimental modal analysis was employed to determine the resonance frequencies of the probe. Subsequently, the probe was pushed into granular materials, both with and without the bending vibrations, by a linear actuator. Experimental results indicated that employing bending vibration in one direction led to a reduction in penetration force by up to 27% while utilizing two directions resulted in a reduction of up to 42%. Additionally, when the probe stopped penetrating the soil due to insufficient axial force, bi-directional bending vibration proved more effective in swiftly fluidizing the surrounding soil. These findings highlight the efficacy of bending vibrations in compact subsurface drilling tools.

* Author to whom any correspondence should be addressed.

Original Content from this work may be used under the terms of the Creative Commons Attribution 4.0 licence. Any further distribution of this work must maintain attribution to the author(s) and the title of the work, journal citation and DOI.

© 2024 The Author(s). Published by IOP Publishing Ltd

Keywords: soil drilling, subsurface investigation, lateral vibrations, resonance frequencies, granular material, lunar regolith, extraterrestrial bodies

1. Introduction

Access to dusty sub-layers of celestial bodies, such as the Moon, Mars, and asteroids, is crucial for scientists and engineers to discover evidence of life and investigate the extraterrestrial past climate, evolution, and resources. Furthermore, the Moon and Mars sublayers' thermal, physical, and mechanical properties have always been vital for scientists to plan early construction and mining activities. Therefore, probes that can penetrate deeper into the sublayers have significant scientific and exploratory value. However, the current conventional subsurface investigation instruments used on Earth, such as rotary or percussive drilling techniques (cone penetration test, pressuremeter test, etc), do not meet the space exploration mass and volume restriction requirements. The rigs used in these investigation instruments penetrate the desired depth by using the high axial force exerted by heavy machinery to overcome the soil layers' resistance. Accordingly, the development of innovative light, compact, and energy-efficient subsurface investigation tools for space missions is of paramount importance.

Numerous investigations have been done to replicate functional principles from organisms such as earthworm, caecilian, and razor clam locomotion, to provide sufficient penetration for a probe. For instance, Omori *et al* (2012) developed a prototype subsurface robotic system consisting of excavation and propulsion units. The excavation unit is based on an earth auger (EA), digging and making a space for the probe to proceed. The propulsion unit was based on the peristaltic crawling of earthworms, which prevents the probe's deviation, keeps it in the vertical position, and adjusts the friction against penetration. After the EA unit creates a hollow volume in front of the probe, the peristaltic crawling mechanism drives it forward. The performance of the prototype under its weight was satisfactory, up to 430 mm in depth. However, more development is needed to remove the dust properly. On another front, inspired by the dual-reciprocating drilling method (DRD) in wood wasp ovipositors, Gao *et al* (2007) designed a bio-inspired micro-penetrator concept, less than 10 kg, consisting of an aftbody and forebody. After ground impact, which was expected to occur at approximately 150 m s^{-1}, the forebody penetrates below the surface while the aftbody remains on the surface for communication purposes. By employing Young's empirical equation, they roughly estimated that the initial penetration would be around 0.6 and 1.3 m, depending on the regolith characteristics. Then, the DRD self-contained drilling system continues for another meter. Later, there were different investigations on the DRD method to develop it further for soil drilling in space exploration. For example, Pitcher *et al* (2020) introduced a compact, self-contained dual reciprocation oscillation drill to overcome payload constraints. This innovative tool combines a cylindrical cam and dual followers for reciprocating motion, inspired by wood wasp ovipositors, with a double-faced wedge for oscillation, drawing inspiration from fish caudal fins. Its design allows for nuanced control over both reciprocating and oscillating movements, influenced by the cam slope and wedge angle.

Another solution proposed for overcoming drilling challenges in planetary missions involves the use of sonic/ultrasonic vibrations to decrease soil resistance and enhance penetration capabilities. In terms of rock drilling in planetary missions, Sherrit *et al* (2000) introduced a light mechanism called ultrasonic/sonic driller/corer (USDC) to address transportation limitations and drilling in harsh environments. The USDC has three main elements: an ultrasonic transducer, free mass, and a drill stem. The ultrasonic units consist of a piezoelectric stack that creates the ultrasonic waves at the frequency of 20 kHz while always remaining under pressure and compressed between a backing element and a horn. The ultrasonic horn has a variable cross-section and is designed to magnify the longitudinal vibration of the piezoelectric stack and transfer it to the free mass. As a result, the free mass starts to vibrate with average frequencies between 100 and 1000 Hz between the tip of the ultrasonic horn and the drill stem. Subsequently, the drill stem transmits the sonic shock waves at the bit/rock interface to the rock, and fracture occurs when fatigue strength is finally passed by hammering. The efficiency of the prototype led to mounting it on several rover configurations (Sojourner Rover and FIDO Rover) and conducting more tests. Although the prototype weighed only 450 grams, it was capable of shallow-depth drilling into different rocks such as granite, diorite, basalt, and limestone with a maximum preload of 5 N and power of 5 W (Bar-Cohen *et al* 2001). A number of studies were later conducted to enhance the method and increase the drilling efficiency. For instance, Cardoni *et al* (2010) designed two new ultrasonic drilling systems for rock sampling, which designed a horn to transfer the longitudinal vibrations into the composite longitudinal-torsional vibrations. They found that the composite mode devices enhanced drilling/coring performance. Wang *et al* (2018) developed a Rotary-Percussive Ultrasonic Drill (RPUD) intended for rock sampling in minor planet exploration. In contrast to previous ultrasonic rock driller designs, RPUD could exploit longitudinal vibrations generated by piezoelectric ceramics on both sides. In addition to the ultrasonic horn, which transfers the longitudinal vibration to the free mass, a V-LT coupler of the rotary unit on the other side of the piezo-ceramics transforms the longitudinal vibration into longitudinal-torsional vibration, which creates an elliptic trajectory on the top of the V-LT coupler. This elliptical motion drives the rotor to rotate continuously by friction on the contact surface. The RPUD prototype requires a driving frequency of 19.95 kHz, a voltage of 225 V_{pp}, and

a preload of 18 N. It can operate at the maximum speed of 117.75 rpm and provides a maximum torque of 38 mNm. They reported that the RPUD prototype has much better drilling efficiency than percussive drilling. While the RPUD prototype drilled 22 mm in 5 min and could exceed this value, percussive drilling could only reach the depth of 15.5 mm in 5 min, while further drilling appeared to be inefficient and almost unlikely.

Regarding penetration testing in regolith and granular materials, Firstbrook *et al* (2014) investigated the effects of high-powered ultrasonic longitudinal vibrations on assisting penetration into granular materials. They used an ultrasonic Langevin transducer to provide ultrasonic vibration of 20 kHz up to 10 μm amplitude. A major limitation comes from the design of the ultrasonic horn penetrator, which must amplify the vibration amplitude and penetrate into the granular materials. The horn attaches to the ultrasonic transducer, and then its cross-section must be reduced to concentrate the vibration and increase the amplitude of the vibration. Therefore, only the lower cross-section area of the horn can penetrate, while the rest remains above the surface. To have a 20 cm length of penetration, they designed the horn from 94Ti/6Al/4V alloy to resonate in the second longitudinal mode at 20 kHz with the resulting amplification ratio (gain) of 3.5. They conducted various penetration tests for Martian regolith simulants with different relative densities. A linear actuator was used to provide the penetration at a slow rate of 3 mm s^{-1} with an input voltage of 4.81 V and a faster rate with a speed of 9 mm s^{-1} with an input voltage of 12 V. Almost in most of the non-ultrasonic penetration tests, they reported a higher penetration force for the slow rate. However, they noticed that the slow rate required a lower penetration force in the ultrasonic penetrations. Moreover, the reduction in the required penetration force was evident in the ultrasonic penetrations. This reduction was more conspicuous in the higher relative density regoliths. Therefore, the ultrasonic technique seems to be useful for assisting penetration into the lunar regolith, which has a high relative density just a few centimeters below the surface. Also, they observed the maximum rate of reduction in the penetration resistance occurred when they increased the amplitude of vibration from 0 to 1 μm, corresponding to the minimum power consumption (actuator and ultrasonic units). After that, the reduction in penetration force was less conspicuous, indicating that the ultrasonic energy had already fluidized the surrounding regolith near the horn's tip, and expanding the fluidized region became more challenging after a certain point.

In order to examine the effect of gravity in ultrasonic penetration, Firstbrook *et al* (2017) conducted a series of penetration tests inside a centrifuge. The tests were conducted in high gravities from 1 g to 10 g, which allowed them to detect a trend and extrapolate the results for lower gravities. Since their previous study examined the effect of penetration rate and a wider range of ultrasonic vibration amplitude (0–5 into various Martian regolith, in this study, they only used one regolith simulant, a medium-fine sub-rounded quartz-based sand (BP) with a density of 1.79 g/cc, the penetration rate of 9 mm s^{-1} with the amplitude range of 0–1.6 μm) in other to focus more on the effect of gravity. They reported higher penetration resistance in higher gravities, while ultrasonic penetration exhibited a higher percentage reduction of the resistance force in lower gravities. For instance, they observed an 80% reduction in penetration force at 1 g in comparison to 70% at 5 g by applying the amplitude of vibration of 1.6 μm. Subsequently, Firstbrook *et al* (2018b) examined the ultrasonic effects on percussive penetration into two regolith simulants. They noticed the number of required strikes to penetrate 190 mm was reduced from 48 to 15 and from 33 to 17 for BP (D_r =48.3%) and SSC-3 (D_r =43.1%), respectively, when they synchronized the ultrasonic vibration pulses with the amplitude of (1.6 μm) with the hammer impacts. Furthermore, they reported that the probe sunk into the granular material for a short time at the beginning of the penetration when they only implemented the ultrasonic vibration. They did not observe this effect at the larger depths of penetration. Finally, (Firstbrook *et al* 2018a) studied the effects of ultrasonic longitudinal vibrations on assisting rotary penetration of an auger drilling rig into glass microspheres with a particle size distribution of 150–250 mm. They noticed that not only the ultrasonic vibration effects are lower than the rotation effect in reducing the maximum overhead force, but it also has no apparent result in reducing the maximum penetration force in rotary drilling. However, they observed that increasing the amplitude of vibration decreased the required maximum torque of 120 Nm in non-ultrasonic rotary drilling to 85 Nm (30% reduction) in ultrasonic rotary drilling with the amplitude of 10 μm.

In the reviewed literature on longitudinal vibration applications, penetration is limited to the horn's tip up to where its cross-section increases and it connects to the ultrasonic transducer. Typically, the cross-section at this connection point between the transducer and the horn is similar, with the horn narrowing towards the tip. This tapering, a common feature in existing ultrasonic systems, is designed to efficiently transmit and focus the ultrasonic waves. Therefore, this design restricts full probe penetration into soil sub-layers. Moreover, despite existing research on high-power longitudinal vibrations, biological locomotions like those observed in snakes, horned lizards (Sherbrooke and Nagle 1996), and sandfish (Baumgartner *et al* 2008) leverage low-frequency bending vibrations for digging or hiding in granular materials. Additionally, Alaei Varnosfaderani *et al* (2022) demonstrated through the discrete element method simulations that lateral vibrations at higher frequencies or amplitudes significantly reduce penetration force in granular materials. However, these simulations assume a rigid probe structure, indicating a need for further exploration of bending vibrations' effects.

Therefore, inspired by the bending vibration of biological locomotions in granular materials, our study aims to experimentally investigate the influence of bending vibration across various resonance frequencies in assisting penetration. Inducing bending vibrations in a structure can be efficiently achieved by applying AC voltage to thin piezo actuator patches on the structure's surface (Dimitriadis *et al* 1991, Dosch *et al* 1992). Accordingly, we excited bending vibrations by attaching thin piezo patches to the machined surface of

the probe structure without expanding its outer dimensions. Also, it is possible to attach the piezo patches inside the probe surface. This approach allowed us to fully bury the entire probe-actuator system into granular materials for practical applications.

2. Experimental apparatus

In this study, we have designed and fabricated a circular probe-actuator configuration to study the effects of bending vibration on soil resistance against probe penetration. Detailed explanations of each component and element of the test setup are provided in the following. First, we described the main components that are shared between different rig penetration tests. Next, we showed the probe configuration. Then, we explained our modal test setup. Finally, we presented the specifications of the granular material used in this investigation.

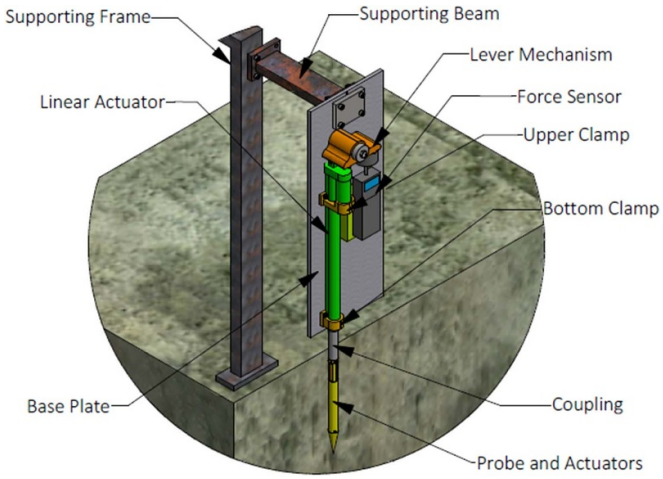

Figure 1. The force and sensor set-up.

2.1. Main components

Figure 1 shows the schematic of the penetration test setup. The linear actuator is connected by a coupling to the probe assembly and pushes the probe into the soil. The required input voltage is 12 V DC, and the maximum speed is 10 mm/s. By reducing the input voltage, we can decrease the penetration speed. The lever mechanism, designed and fabricated using three-dimensional (3D) printing technology, is positioned between the force sensor and the linear actuator. The sensor, linear actuator, and lever mechanism are installed on a base plate. The supporting beam holds the base plate and is connected to our laboratory's fixed supporting frame. The clamps are also printed with the 3D printer, and they are designed only to prevent falling and side movements of the linear actuator-probe assembly.

2.2. Rigs configuration

Figure 2 illustrates the configuration of the probe-coupling assembly and the positioning of the piezo patches on the Aluminium probe. More detailed drawings have been provided in the appendix. In our approach, we have machined the outer surface of the probes to facilitate the attachment of the piezo patches. These patches are thin and, when glued to the machined surface, do not increase the overall perimeter of the probe. This design allows us to push the probe and piezo patches together into the soil. However, to safeguard the piezo patches from potential contact and wear caused by the soil, we limit the insertion depth to 24 cm. It is important to note that, for practical implementation, it is possible to securely place the piezo patches inside the tube using advanced machining and manufacturing techniques. This ensures their protection from direct contact with the abrasive granular materials. The piezo patches used in this setup have dimensions of 49.7 mm $\times$ 7. mm $\times$ 0.80 mm, and they are made from PZT material (No. 850 (APC International, Ltd. 2021)). In figure 2(b), the cross-sectional areas of the piezo patches attached to the machined surface of the probes and their polling directions are shown. We utilized two sets of piezoelectric patches placed on parallel machined surfaces. In each set, the piezo patches have the same poling direction.

Figure 3 displays how electrical circuits are employed to generate bending vibrations in various directions within the probe structure. By applying an AC voltage to the outer electrodes of a specific set of piezo patches, we can induce one-directional bending vibration in the structure. This vibration occurs parallel to the polling direction of that particular set of piezo patches. It's essential to maintain a ground connection at the interface between the probe and the piezo patches to carry out this process. In figures 3(a) and (b), the required electrical circuits for generating unidirectional bending vibrations are presented, with the vibration direction indicated in each figure. In addition, we can create chaotic bending motions or whirling motions if we use the electrical circuit illustrated in figure 3(c). Applying an AC voltage to the outer electrodes of one set and another AC voltage (with a different frequency) to another set and grounding inner electrodes induce complex bending motions in two directions within the probe structure. This results in a chaotic horizontal movement at the tip of the probe. However, if the second signal has the same frequency as the first one but with a precise phase difference of 90 degrees, the bending vibrations in two directions generate a circular whirling motion in the probe structure and at its tip.

2.3. Signal generator and data acquisition system

Our signal generator and data acquisition system is a four-channel Siemens LMS SCADAS mobile integrated with LMS Test Lab software. Figure 4 shows the schematic of our modal test. The signal generator creates the required AC voltage, and it will be applied to the piezoelectric actuators attached to the probe structures. The input signal can be generated by either our LMS software or 33 120A Agilent Arbitrary Waveform

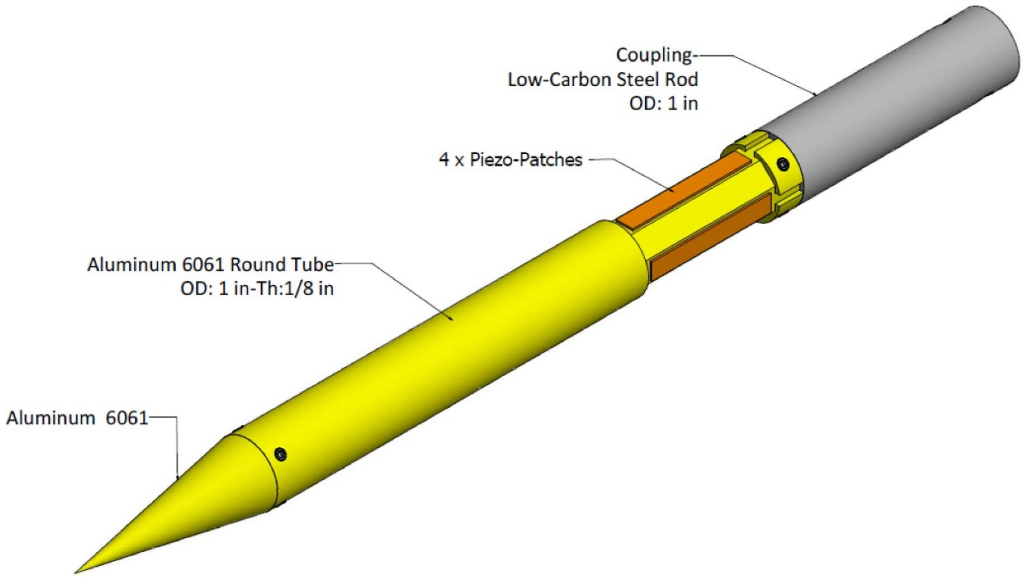

(a) Probe coupling Assembly

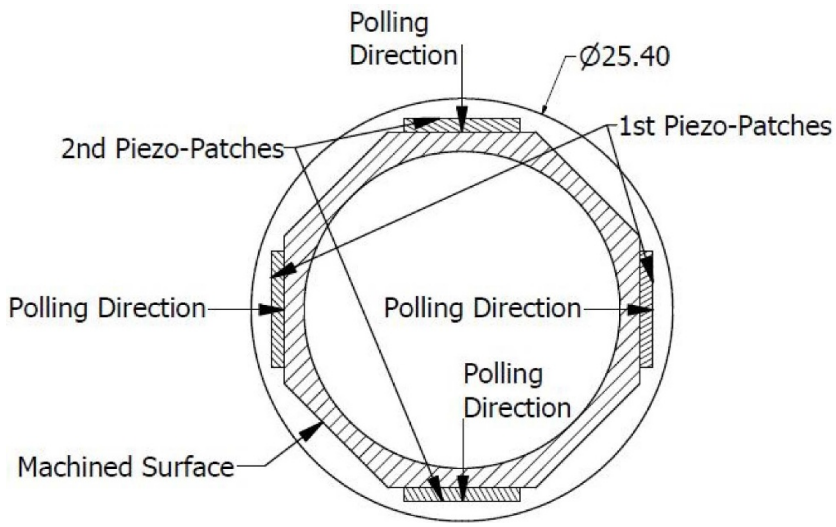

(b) Probe actuators configurations

Figure 2. Probe configuration.

Generator. The applied voltage creates vibration in the probe structure. To measure the resulting lateral velocity at the probe tip, we used a laser vibrometer sensor. This sensor consists of a Polytec OFV-5000 Vibrometer controller and a Polytec OFV-505 Vibrometer Sensor Head. The sensor head detects the lateral velocity and provides a corresponding voltage signal, which is then transmitted to the data acquisition system. Finally, the LMS Test Lab software shows and saves all the input voltage signals and the recorded velocities.

In the penetration test, the resonance voltage signal(s) generated by the signal generator will be amplified through the amplifiers to reach $V_{\max} = 200\,\mathrm{V}$. Then, the amplified signals will be applied to the piezoelectric actuators.

2.4. Soil Properties

The soil sample consists of fine-cutting sub-angular limestone particles, as shown in figure 5 with the maximum and minimum dry density of $1950\,\mathrm{Kg\,m^{-3}}$ and $1610\,\mathrm{Kg\,m^{-3}}$, respectively. The limestone sample contains particles, with nearly 60% of its weight having particles finer than 0.42 mm.

In order to ensure the proper mixing of granular particles to achieve a homogeneous distribution and obtain consistent results, it is recommended to pour the material from a height greater than 40 cm, as stated by Firstbrook *et al* (2014). Taking this into account, we have devised a setup consisting of a container with a built-in cone, a stand, and a steel pail. The container is positioned above the stand, enabling a hands-off

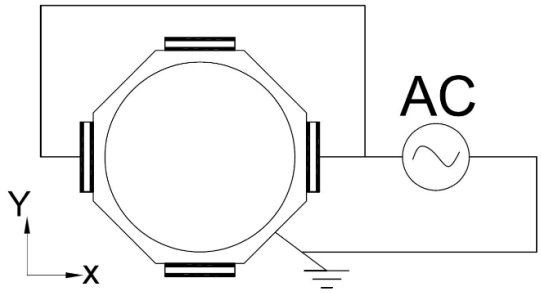

(a) AC Voltage to the first set and vibration in X direction

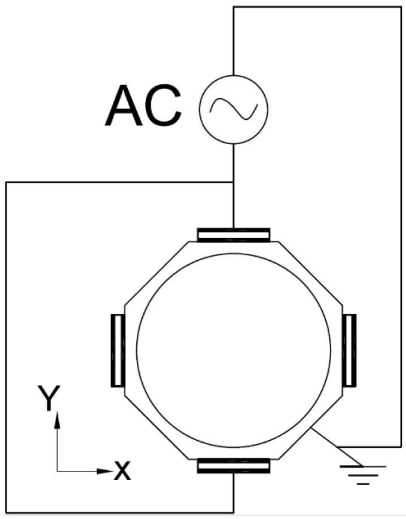

(b) AC Voltage to the second set and vibration in Y direction

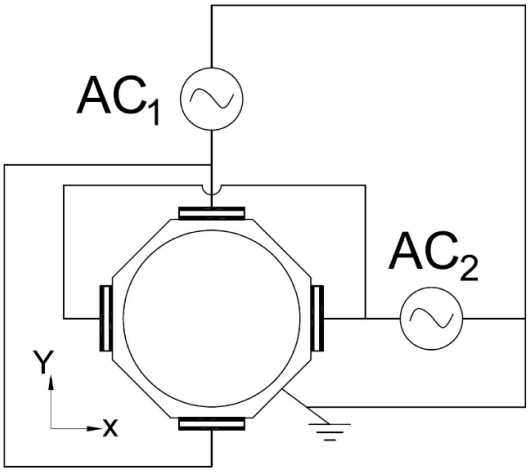

(c) Complex vibration/Whirling motion excitations

Figure 3. Applying voltage and exciting bending vibrations in different directions.

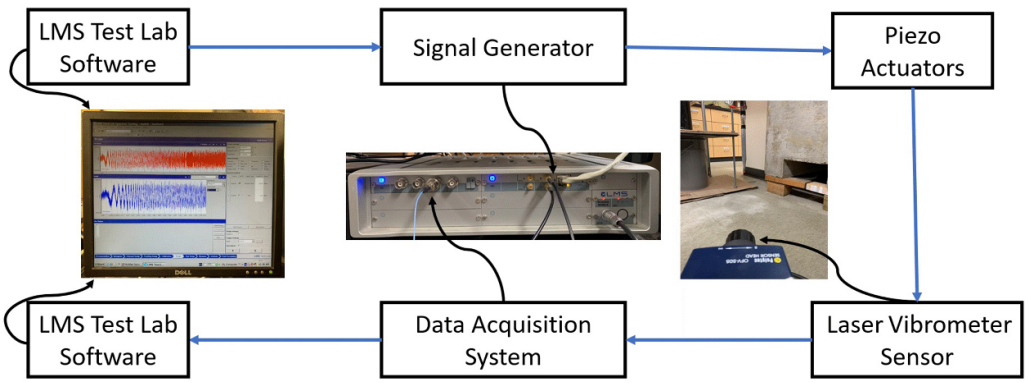

Figure 4. Modal test setup.

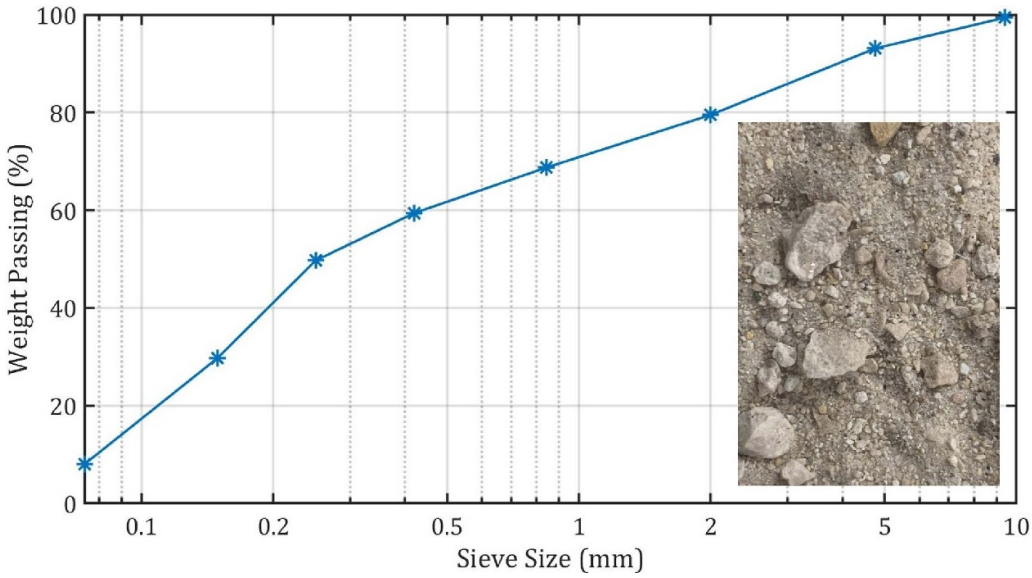

Figure 5. particle size distribution.

pouring of sand into the pail located at the base of the stand (figure 6). The hands-off approach is beneficial for maintaining consistent results. The bottom of the container is positioned approximately 100 cm above the pail to ensure that the granular particles receive a sufficient fall distance. The process results in medium-dense sand with a bulk density of around 1790 Kg m^{-3} and a relative density of 58%. Additionally, the pail used for this procedure has a diameter of 28.8 cm and a height of 40 cm. It is worth noting that the pail's diameter is over 11 times larger than the diameter of the probe to ensure minimal boundary effects during the penetration tests, as noted by Bolton *et al* (1999).

3. Experimental procedure and results

In this section, we begin by presenting the penetration test results for the non-vibrating probe. Following this, we conducted modal tests in subsequent sections to identify various resonance frequencies and mode shapes of the probes. Subsequently, rapid penetration tests were performed to pinpoint the most promising and beneficial resonance vibrations for penetrations. Finally, we present and discuss a series of penetration tests that utilize the most effective resonance modes to reduce the required vertical force for penetrating the probe.

3.1. Non-vibrating probe penetration tests

Figure 7 displays the recorded forces of three consecutive tests performed on undisturbed samples without applying any vibration (non-vibrating probe) along with the average (AVG) penetration forces for these three tests. As can be seen, there

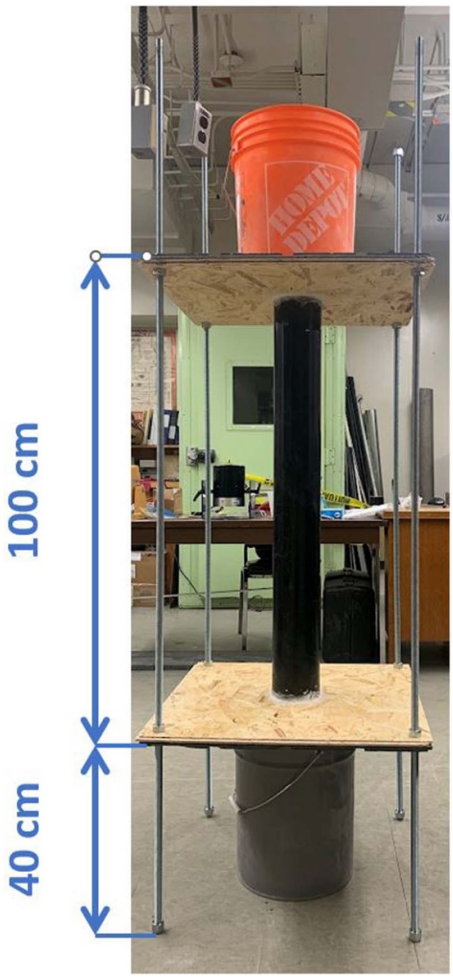

Figure 6. Hands-Off Approach to Pouring Sand into the Pail.

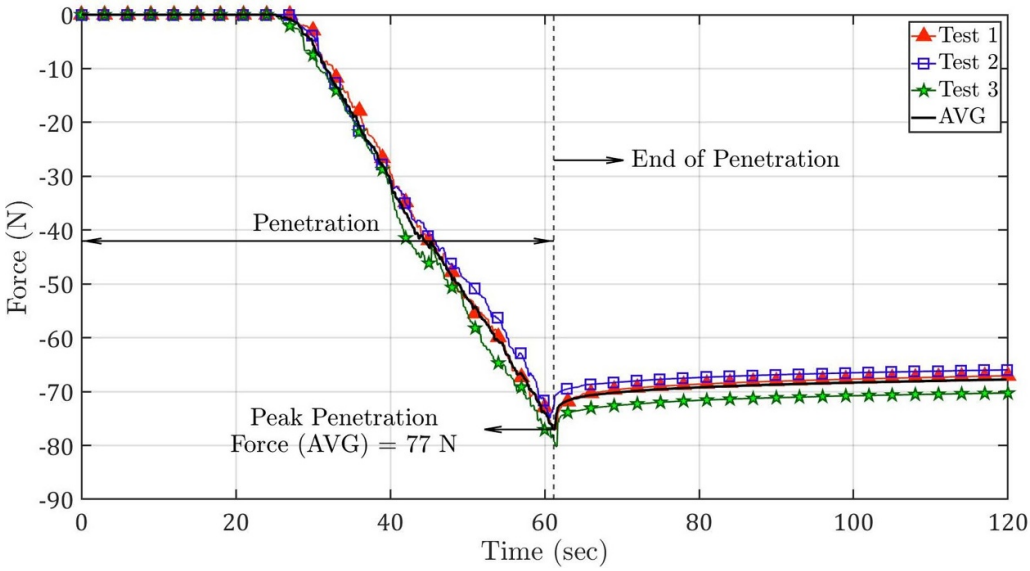

Figure 7. Penetration force of non-vibrating probe.

is a distinct peak in the magnitude of the recorded penetration force precisely when the linear actuator terminates the penetration process at around 61 s. Throughout the actuator's operation, a slight deflection in the frame was observed. It was expected that the penetration force would drop to zero immediately when the linear actuator stopped working. However, the deflected frame caused the recorded penetration force to drop only slightly to a semi-steady state. In fact, upon stopping the linear actuator at the end of penetration, the deflected frame shape pushed the probe into the soil to return to its initial shape and release stresses. However, as the penetration force from the deflected frame was insufficient for an immediate complete return, the frame remains deflected, leading to a very gradual reduction in the recorded force and the observation of a semi-steady state. The penetration process typically lasts for about 61 s, with a penetration rate of 4 mm s^{-1} for all tests. For the non-vibrating probe penetration (figure 7) and the subsequent tests with the vibrating probe (3.5), we extended our recordings to 120 s. This extension enables us to assess the impact of bending vibration on two aspects: first, the reduction in penetration force as the probe penetrates the soil (prior to $t \approx 61$ s), and second, the damping of the peak force when the linear actuator stops (beyond $t \approx 61$ s).

It's worth noting that the recorded forces remain at zero for the approximately initial 25 s in figure 7. During this period, as the linear actuator is extending, the combined weight of the probe and actuator is sufficient to drive the probe into the soil sample. Beyond this point, the probe can no longer advance based on its own weight alone. Therefore, the linear actuator provides the extra required force, which is supported by the lever mechanism, and recorded by the force sensor.

Additionally, the maximum deviation in peak force from the average curve is approximately 4% (figure 7). Moreover, when the system reached the semi-steady state at $t = 120$ s, the deviation was less than 4%. In 3.5, we employed this average plot for comparative analyses with the penetration forces in the presence of bending vibrations.

3.2. Modal analysis

In the modal tests, we applied a chirp signal to each set of actuators separately to measure the velocity of the probe tip and identify its bending vibration resonance modes. The chirp signal had a maximum voltage of $V_{max} = 10$ V, with the frequency sweeping from 10 Hz to 20.480 kHz (the maximum frequency of the signal generator). The spectrum diagram of the input signal is depicted in figure 8.

For each set of piezoelectric patches, we began by exciting the piezoelectric in front of the laser vibrometer sensor (figure 9(a)). This induced a bending vibration with waves traveling on one side of the probe. Subsequently, we activated the second piezoelectric patch in the same set, producing a similar bending vibration pattern on the opposite side (figure 9(b)). Lastly, both piezoelectric patches were activated simultaneously, leading to a combined vibration effect (figure 9(c)). This entire process was then repeated for the second set.

Figure 10 displays the amplitude spectrum of the probe tip's speed in two distinct directions. The first direction corresponds to the activation of the first set of piezo actuators, while the second direction, perpendicular to the first one, corresponds to the activation of the second set of piezo actuators. The directions 1 and 2 here are correpsponding the X and Y directions shown in figure 3. Figure 10(a) shows the results for the first direction, while figure 10(b) is related to the second direction. Both figures 10(a) and (b) demonstrate that when a single piezoelectric patch is active in a set, the responses at the probe tip are quite similar to when the other patch is active alone in the same direction. Additionally, exciting both piezoelectric patches simultaneously approximately doubles the vibration

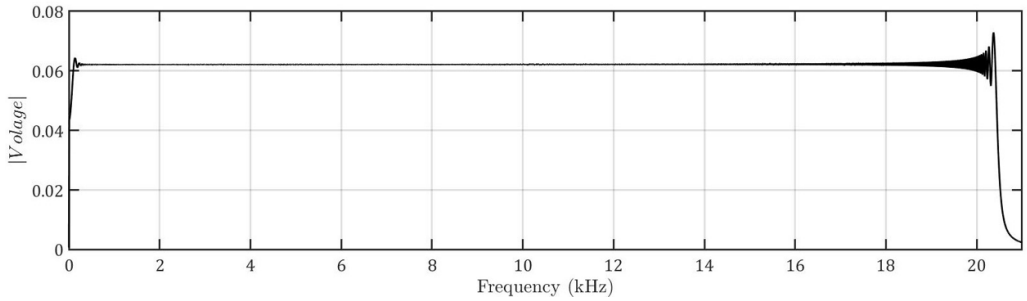

Figure 8. Single-sided amplitude spectrum of the input voltage.

speed in each direction. This consistent outcome is a result of the similar properties of the piezoelectric patches and also indicates a reliable and consistent bond between the patches and the probe.

It's worth noting a slight difference in the natural frequencies between the two directions. For example, we have a bending resonance mode of $f_1 = 6069$ Hz in the first direction, and this mode is $f_2 = 5886$ Hz in the second direction. In an ideal scenario, symmetrical probes would have the same resonance frequencies for similar bending modes in both directions ($f_1 = f_2$). However, small differences due to manufacturing or gluing the piezoelectric patches can lead to slight frequency deviations. At higher resonance frequencies, like around 9405 kHz, the differences in vibration become more noticeable. This is probably because the higher the frequency, the more these vibrations are affected by small imperfections or inconsistencies in how the piezoelectric patches are attached and the probe's overall symmetry. To simplify, when we discuss a specific bending mode regardless of its direction, we represent it with its corresponding average frequency (e.g. bending mode at $f_{\text{avg}} = 5978$ Hz refers to bending modes $f_1 = 6069$ Hz in the first direction and $f_2 = 5886$ Hz in the second direction).

After recording the velocity, we further transformed it into displacement and acceleration measurements. Figure 11 illustrates the FFT of the probe tip's displacement, velocity, and acceleration. Upon observing figure 11(c), it becomes evident that the acceleration of the probe's tip is not notably prominent below 3000 Hz when compared to the broader frequency range of 3–20 kHz. Furthermore, figure 11(a) indicates the displacement of the probe's tip remains minimal above 10 kHz (within the 10–20 kHz range) compared to the rest of the probe tip's frequencies (0–10 kHz). Consequently, we can reasonably estimate that the most effective resonance modes for fluidizing the sand are most likely situated within the frequency range of 3–10 kHz. This range exhibits notably higher levels of both displacement and acceleration compared to the entire frequency spectrum.

3.3. Preliminary penetration tests

Initially, our objective is to identify bending resonance modes that can fluidize the soil sample for subsequent primary penetration tests. We used the linear actuator to push the probe into the soil at various depths to achieve this objective. When the penetration process stops, the force in the structure does not drop to zero due to the slight deflection of the frame, and the force sensor indicates that the probe is under compression. Following this, we used an amplifier to apply a voltage of $V_{p-p} = 400$ V at various resonance frequencies to the piezo patches. If a bending resonance frequency proves effective in fluidizing the soil, the stress in the structure is released, resulting in a decrease in force as indicated by the force sensor. Our findings revealed that resonance frequencies below 3000 Hz have no noticeable effect on soil fluidization and are ineffective in reducing the force in the force sensor. This is because the acceleration amplitude at frequencies below 3000 Hz is very low when compared to the rest of the frequency range. Acceleration plays a crucial role by imparting enough inertia force to the soil particles, allowing them to shift away from the probe's tip. On the other hand, within the 10–20 kHz range, even with the high level of acceleration of the probe tip compared to the other resonance modes in the whole frequency range, only vibrations at 13 250 Hz showed limited potential in our preliminary penetration tests to reduce the penetration force. This can be attributed to the amplitude of displacement at a frequency range of 10 000 Hz–20 000 Hz, which is very low compared to the resonance modes between frequencies of 0–10 kHz. The amplitude of displacement needs to reach a significant level to effectively transfer the vibration energy to the soil particles, as pointed out by Alaei Varnosfaderani *et al* (2022). Conversely, resonance frequencies of $f_1 = 3626$ Hz, $f_1 = 6069$ Hz, and $f_1 = 9688$ Hz along the direction 1 noticeably reduced the force to zero, indicating their effectiveness in soil fluidization. This is because the resonance frequency within the 3–10 kHz range demonstrates significantly higher levels of both displacement and acceleration when compared to the entire frequency spectrum. Therefore, these frequencies have been selected for the main penetration tests. Also, for inefficient modes, we chose 1554 Hz and 13 250 Hz as they exhibit the highest acceleration below 3000 Hz and above 10 000 Hz, respectively. Additionally, 13 250 Hz showed slight potential for soil fluidization.

3.4. Finite element analysis (FEA)

In our study, FEA was employed to model the experimental setup using ABAQUS in order to visually demonstrate the

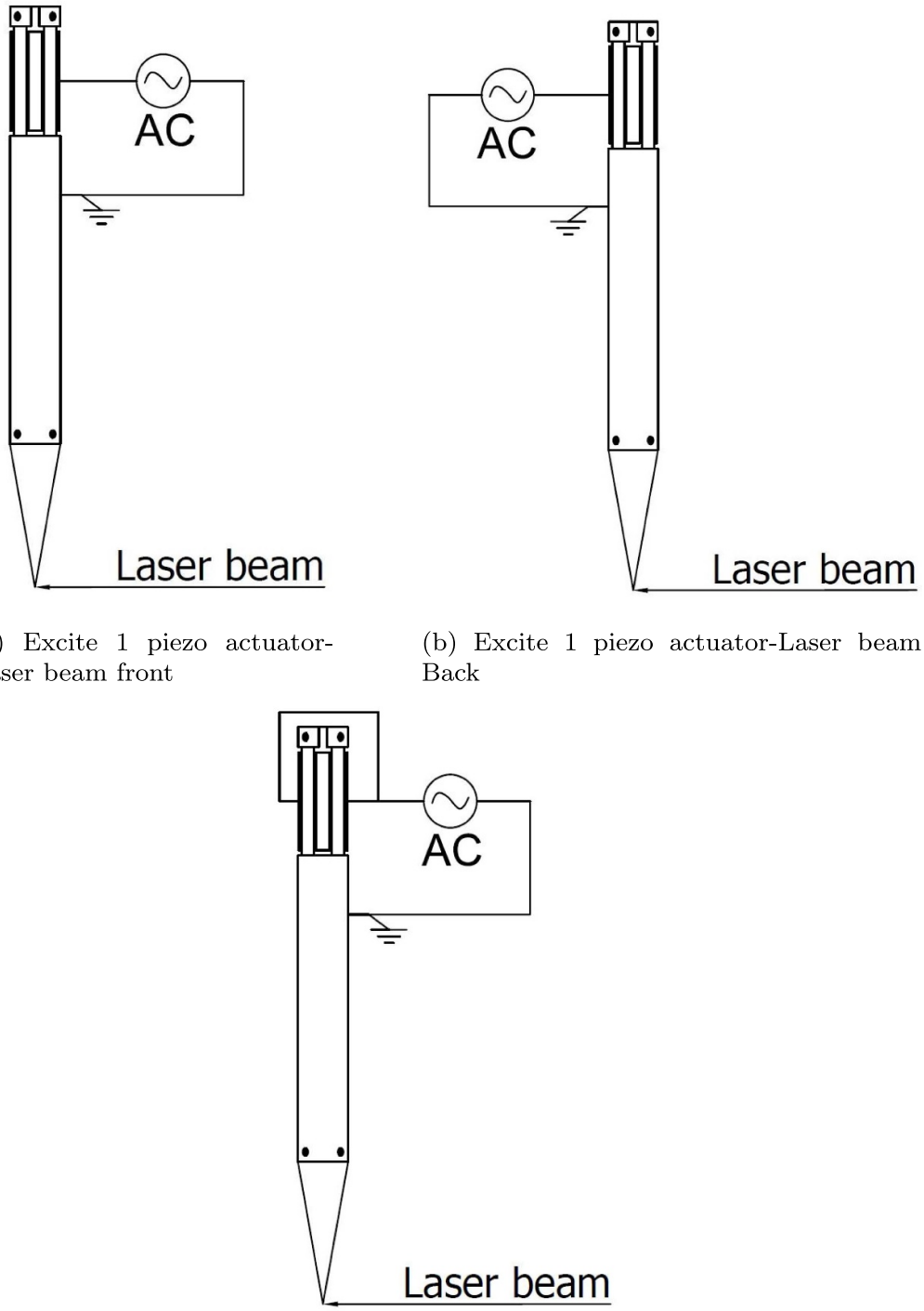

(a) Excite 1 piezo actuator-Laser beam front

(b) Excite 1 piezo actuator-Laser beam Back

(c) Excite 2 piezo actuators together

Figure 9. Bending vibration and laser beam direction.

specific mode shapes that we excite during soil penetration tests. The model included several components: the probe itself, the coupling mechanism, piezoelectric patches, and the shaft that connects to the linear actuator. The model was built with 352 804 nodes and 239 394 elements. It utilized 237 082 C3D10 quadratic tetrahedral elements for the structural parts and 2312 C3D10E elements for the piezoelectric patches. The resulting mode shapes are depicted in table 1.

Furthermore, we performed a comparison between the average bending frequencies obtained from the ABAQUS

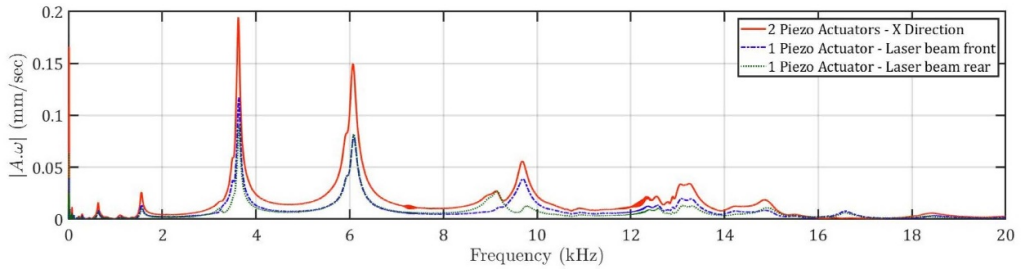

(a) Direction 1

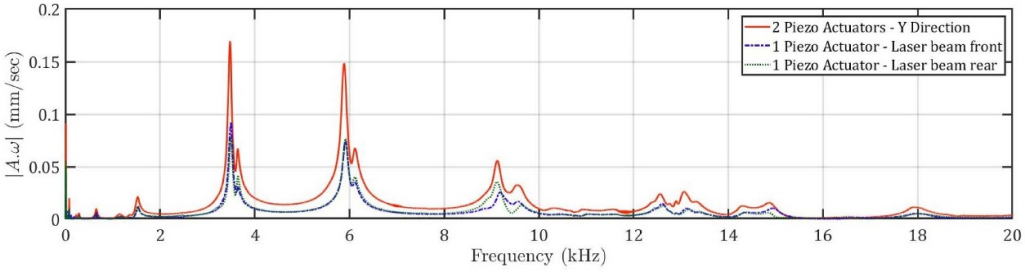

(b) Direction 2

Figure 10. Single-sided amplitude spectrum of probe tip velocity.

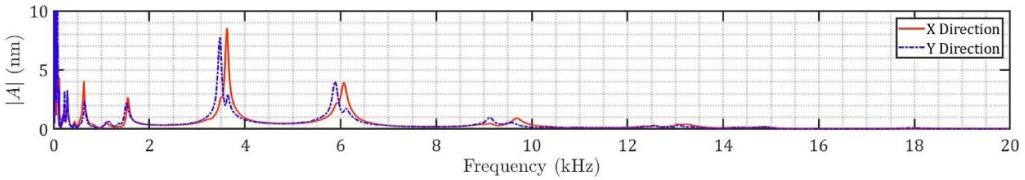

(a) Displacement Amplitude Spectrum

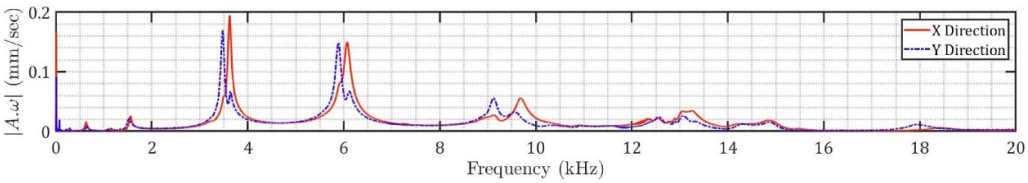

(b) Velocity Amplitude Spectrum

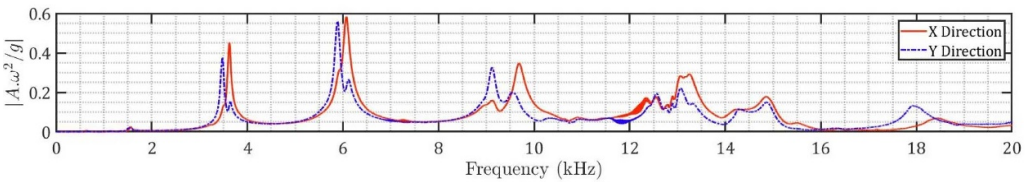

(c) Acceleration Amplitude Spectrum

Figure 11. Single-sided amplitude spectrum of probe tip.

simulations and those measured during our laboratory tests, as shown in table 2.

While our simulation results successfully approximated the natural frequencies and mode shapes, modeling the complex entire system posed significant challenges. The system's dynamic response is influenced by the integrated assembly of the probe, coupling, linear actuator, base plate, supporting beam, and frame, which complicates the simulation. Notably, slight deflections in the support structure during penetration underscored the interconnectedness of system components and their impact on the system's dynamic response. Therefore, FEA was primarily leveraged to illustrate the resonance mode shapes critical for our penetration tests.

3.5. Main penetration tests

3.5.1. Uni-direction Bending Vibration. In this section, we performed diverse penetration tests, recording the necessary penetration force at different frequencies to assess and compare the results with the average penetration forces of

Table 1. Bending mode shapes used for penetration tests.

X direction	Y direction
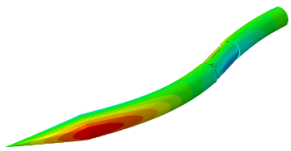	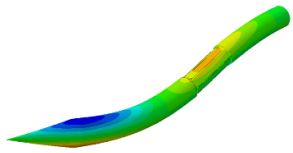
(a) 1541.4 Hz	(b) 1541.6 Hz
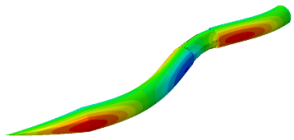	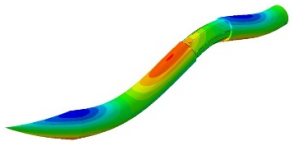
(c) 3037.4 Hz	(d) 3039.0 Hz
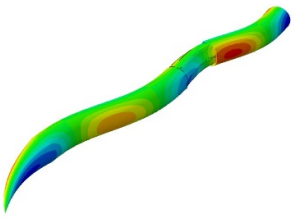	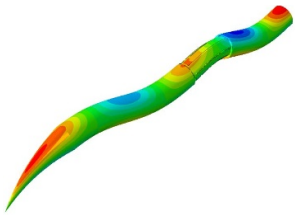
(e) 6256.6 Hz	(f) 6258.3 Hz
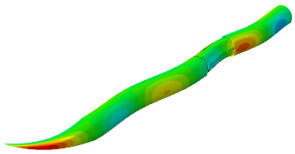	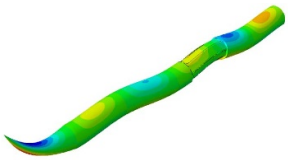
(g) 9797.5 Hz	(h) 9797.2 Hz
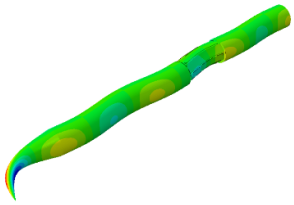	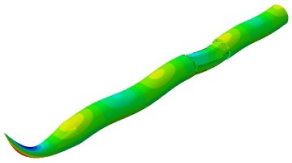
(i) 14055 Hz	(j) 14056 Hz

Table 2. Comparison of average bending frequencies.

AVG from abaqus	AVG from modal tests	Difference %
1541.5	1543	1.0%
3038.2	3553	14.4%
6256.4	5978	−4.6%
9797.3	9405	−4.2%
14 055.5	13 159	−6.8%

the non-vibrating probe in figure 7. As discussed above, figures 3(a) and (b) demonstrate the driving electrical circuit diagram used to induce bending vibrations in the X and Y directions, respectively. Figure 12 compares the penetration force of the probe when it is non-vibrating with the vibrating one at the frequencies of 1554 Hz and 13 250 Hz. Given the anticipated 4% difference in test results, figure 12 indicates no improvement in the peak penetration force at these resonance modes. When the linear actuator is stopped at the end of the penetration (around 61 s) at 13 250 Hz, there is only a minor enhancement in damping the peak force. This slight improvement is likely due to the high acceleration of the probe (figure 11(c)). However, as discussed in 3.3, the bending vibration displacement amplitude at the probe's tip above 10 kHz is not sufficiently large (figure 11(a)). This prevents the efficient transfer of vibrations to the surrounding sand. Furthermore, there is no noticeable improvement in penetration tests at the frequency of 1554 Hz. This lack of improvement is attributed to the insufficient acceleration of the probe tip (figure 11(c)), which fails to provide the necessary inertia for soil particles to initiate movement and fluidization.

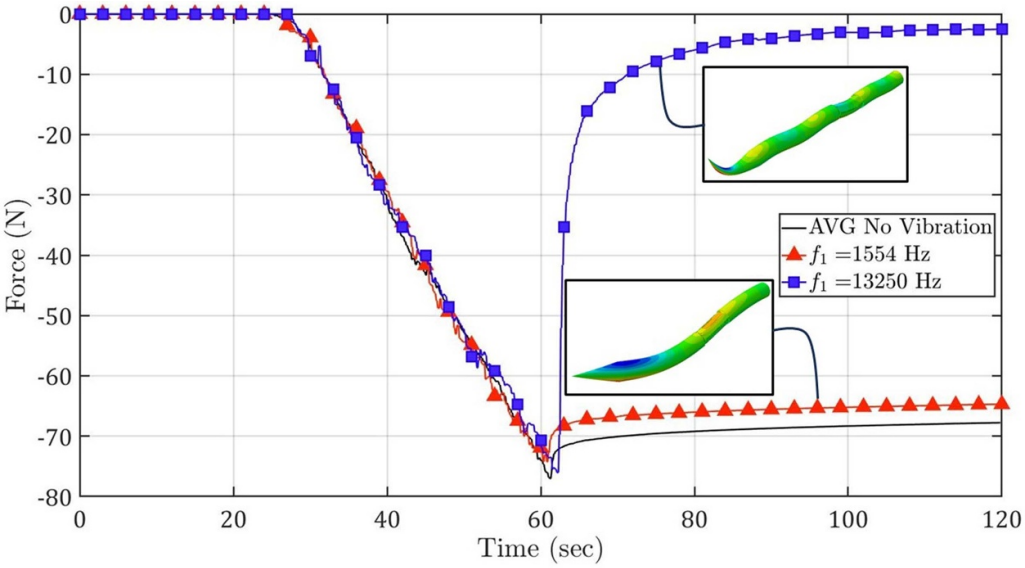

Figure 12. Penetration force with inefficient modes of vibration.

Figure 13 presents a comparison of penetration forces under more favorable bending vibration modes against penetration forces without vibration. Each drawing compares average penetration forces without and with vibration at a specific bending resonance mode. These modes are denoted as f_1 for the first direction and f_2 for the second direction as described in 3.2. The average penetration force at these modes (f_1 and f_2) is also indicated in each figure.

In figure 13(a), the resonance frequencies are $f_1 = 3626$ Hz for the first direction and $f_2 = 3479$ Hz for the second direction. Figure 13(a) indicates that this bending vibration mode had minimal impact on reducing penetration force during the sand penetration process. Notably, they did not significantly affect the maximum penetration force either. However, a significant decrease in the peak force magnitude was observed once the linear actuator ceased its motion. The average curve shown in figure 13(a) indicates that, in this vibration mode, the force took approximately 2.3 s to reach zero after the probe stopped its penetration. In contrast, without vibration, there was only a 12% reduction in peak force at $t = 120$ s (59 s after the probe stopped penetrating). This suggests that this vibration mode could be most advantageous when the probe experiences frequent pauses and restarts or when it moves at a very slow penetration rate.

In figure 13(b), the resonance frequencies are $f_1 = 6069$ Hz for the first direction and $f_2 = 5886$ Hz for the second direction. This figure also presents average penetration forces for these vibration scenarios and the non-vibrating probe. In figure 13(b), resonance frequencies are $f_1 = 9688$ Hz for the first direction and $f_2 = 9122$ Hz for the second direction. For a better comparison with non-vibrating probes, figure 13(d) displays average penetration forces for vibro-probes from figures 13(a)–(c) and to the non-vibratory probe. Moreover, we extract key parameters, including the maximum penetration force ($F_{\max}$), the reduction in maximum penetration force ($R\%$), and the release time ($t_{\max}$) required for the force to drop to zero when the probe stops at the end of penetration, from the findings in figure 13(c). These results are summarized in table 3. Vibration modes at f_{avg} =5915 Hz and f_{avg} =9833 Hz in both directions considerably reduce penetration forces. However, the lower frequency mode ($f_{\text{avg}} = 5915$ Hz) demonstrates a more pronounced reduction. In figure 13, vibrating at $f_{\text{avg}} = 5915$ Hz reduces maximum penetration forces by 28% (from 77 N to 55.5 N) and eliminates the penetration force within 1.15 s. On the other hand, vibrating at $f_{\text{avg}} = 9800$ Hz reduces maximum penetration forces by 21% (from 77 N to 60.8 N), with the peak force dissipating over 4.4 s.

3.5.2. Bi-direction bending vibration. Moving forward, we investigate the effects of bi-directional excitation on the piezo probe with the combination effects of the efficient bending modes. In this approach, we apply an AC voltage to the first set of piezoelectric elements and another AC voltage to the second set (figure 3(c)). The two signals either share the same frequency with a 90-degree phase difference or have different frequencies. As a result, the probes generate bending vibrations in both directions. When the frequencies are similar with a 90-degree phase difference, this results in a whirling circular motion in the probe. Alternatively, if there are two distinct frequencies of bending vibration in each direction, it leads to chaotic motion in the probe. Utilizing the recorded velocity data at the probe's tip (figure 10), corresponding to the input chirp signal (figure 8), we calculated the probe's tip displacement in the XY plane resulting from harmonic excitations in both directions. In the analysis of whirling motion, the excitation frequency for each resonance mode is identified as the average of the resonance frequencies in the X and Y directions. This averaged frequency is then applied to both sets of piezoelectric patches. Figure 14 presents the displacement of the probe tip for the three predominant resonance modes. The resulting trajectory predominantly exhibits an elliptical shape and is within a timeframe of $\Delta t = 3.8 \times 10^{-4}$ s.

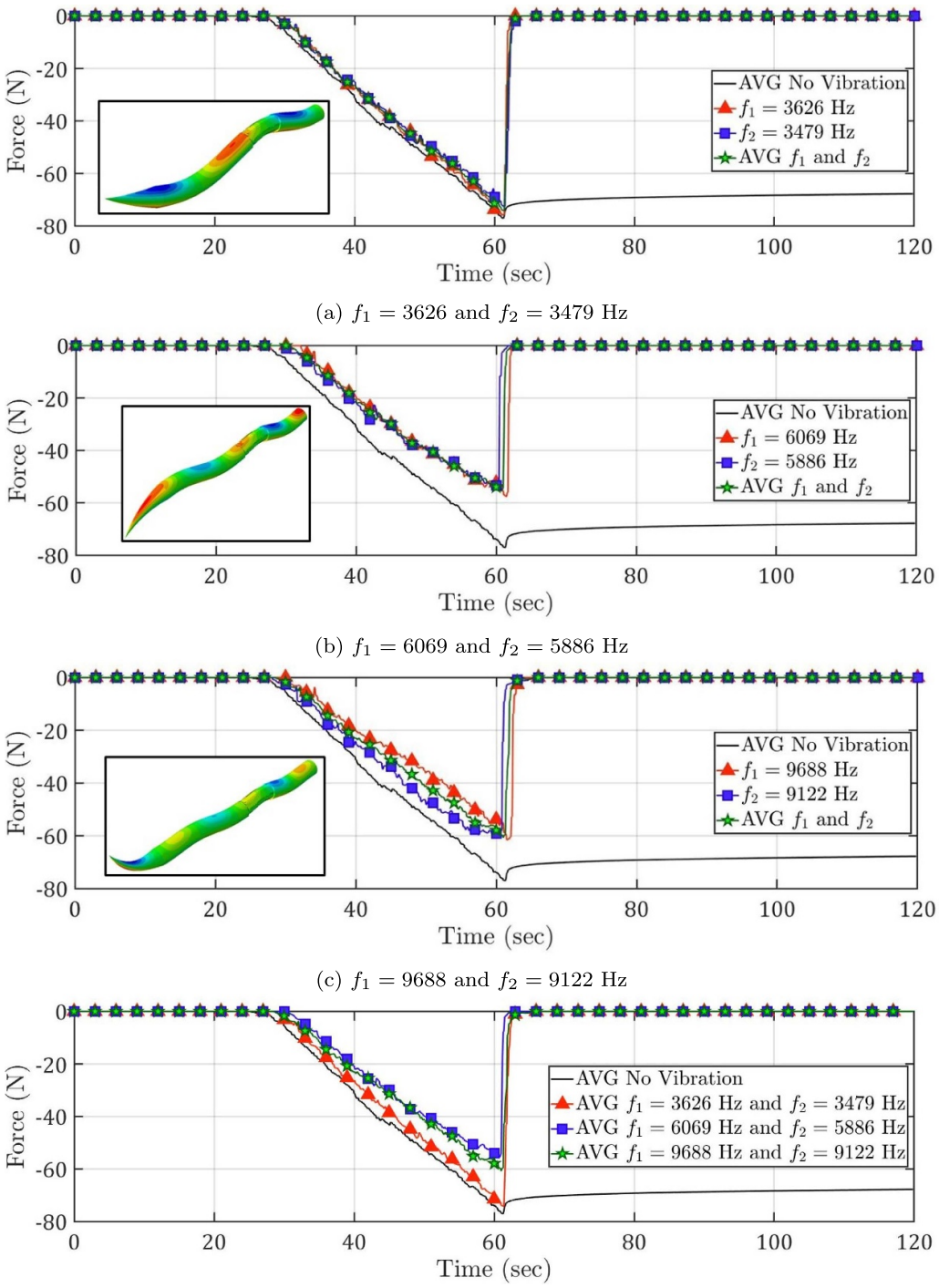

(a) $f_1 = 3626$ and $f_2 = 3479$ Hz

(b) $f_1 = 6069$ and $f_2 = 5886$ Hz

(c) $f_1 = 9688$ and $f_2 = 9122$ Hz

(d) Average penetration force

Figure 13. Penetration force at efficient bending modes.

However, the ellipse's orientation dynamically shifts because the excitation frequency is finely tuned to approximate the average frequency of the two similar bending resonances across different directions. The capacity for the trajectory to change direction offers a significant advantage for penetration, as it allows the probe to uniformly and effectively fluidize the soil in every direction surrounding the probe, thereby facilitating enhanced penetration capabilities.

For the chaotic probe motion, wherein two distinct resonance modes are excited in different directions, the excitation frequency corresponds precisely to the resonance frequency specific to each direction. Therefore, the trajectory of the probe's tips, as depicted in figure 15, exhibits chaotic motion within the *XY* plane, attributable to the differing excitation frequencies. Similar to the whirling motion, such chaotic behavior plays a significant role in fluidizing the soil uniformly

Table 3. Penetration forces in one-directional excitation.

f_{avg} (Hz)	F^{a}_{max} (N)	R^{b}(%)	$t_r{}^{c}$(s)
0	77	—	–
3553	74	4%	2.3
5978	56	28%	1.4
9405	61	21%	4.4

[a] Maximum penetration force in Newton.
[b] Percentage of maximum force reduction.
[c] Release time in seconds.

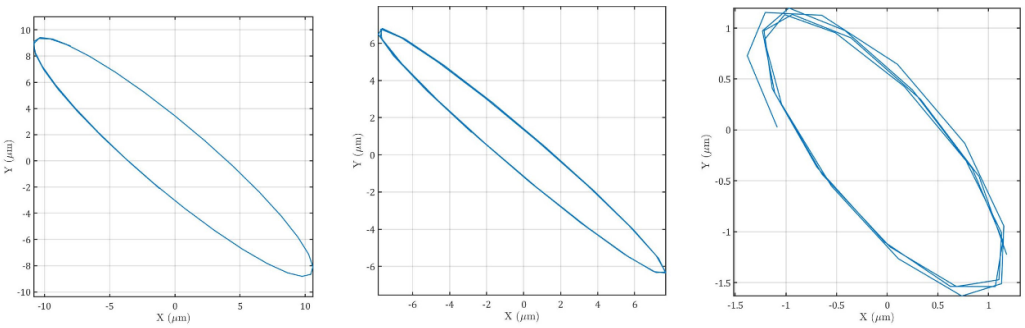

(a) f_{avg}= 3553 (Hz) (b) f_{avg}= 5978 (Hz) (c) f_{avg}= 9405 (Hz)

Figure 14. Trajectories of the probe tip's whirling motion for three effective resonance modes.

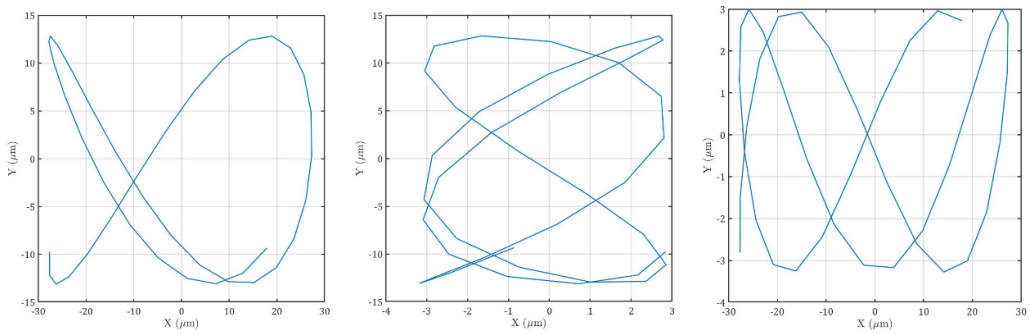

(a) f_1= 3626 (Hz), f_2= 5886 (Hz) (b) f_1= 9688 (Hz), f_2= 5886 (Hz) (c) f_1= 3626 (Hz). f_2= 9122 (Hz)

Figure 15. Trajectories of the probe tip's chaotic motion.

across the *XY* plane and, therefore, increasing the probe's penetration efficiency.

The outcomes for the penetration tests are presented in figure 16. The maximum penetration force and the time when it drops to zero when the probe stops have improved for all three combinations. For a better comparison of the results, we presented them in table 4. When comparing the results of bidirectional excitation (refer to figure 16 and table 4) with unidirectional excitation (see figure 13 and table 3), it is evident that bidirectional excitation significantly reduces penetration forces and accelerates the force drop to zero when the probe stops penetrating.

In unidirectional excitation, a maximum 27% reduction in penetration forces was observed at 5978 Hz. However, bidirectional excitations produced more substantial reductions, ranging from 33% to 42% for chaotic motions and 15%–41% for whirling motions. Notably, the 15% improvement is seen in the 3553 Hz whirling motion, a significant enhancement compared to the 4% reduction with the signal applied in only one direction.

From table 4, it is apparent that the most effective reduction in penetration force occurs with at least 9405 Hz in one direction. The optimal case is when this mode is applied in two directions, resulting in a 42% drop in maximum penetration force from 77 N in the non-vibrating probe to 45 N. The time for the force to drop to zero upon cessation of penetration is reduced to 1 s compared to 4.4 s when applied in one direction. When applying an AC signal with 9405 Hz in one direction and 3553 Hz or 5978 Hz in another direction, the reduction in maximum penetration forces is 42% and 35%, respectively, with release times of 2 s and 0.8 s, respectively.

Table 4 also indicates that the quickest reduction in penetration forces upon the probe's penetration cessation occurs when the frequency is 5978 Hz in at least one direction. For example, the release time is 0.7 s when both directions have 5978 Hz excitation voltage and 0.8 s when one direction has 5978 Hz

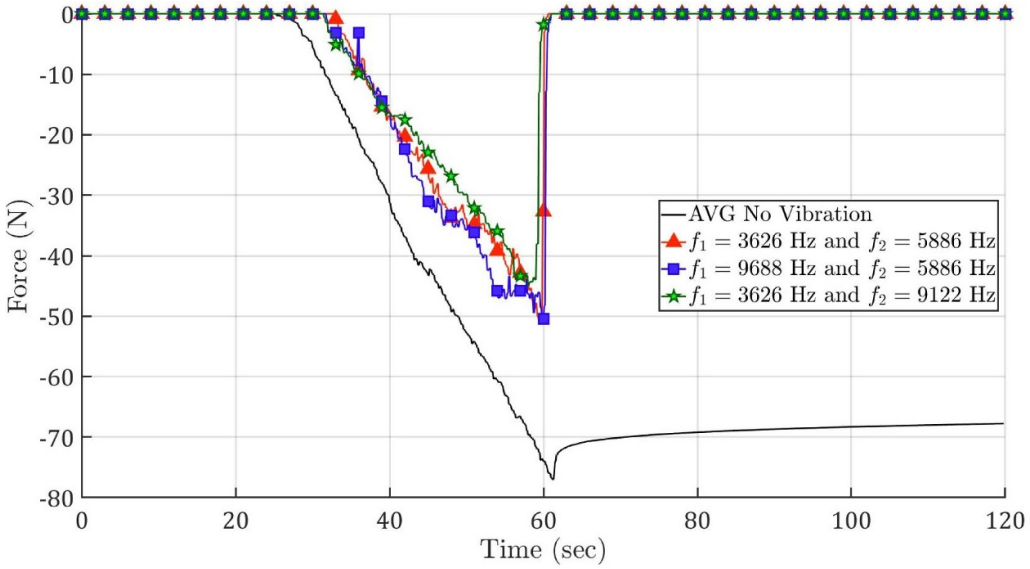

(a) Chaotic probe motion

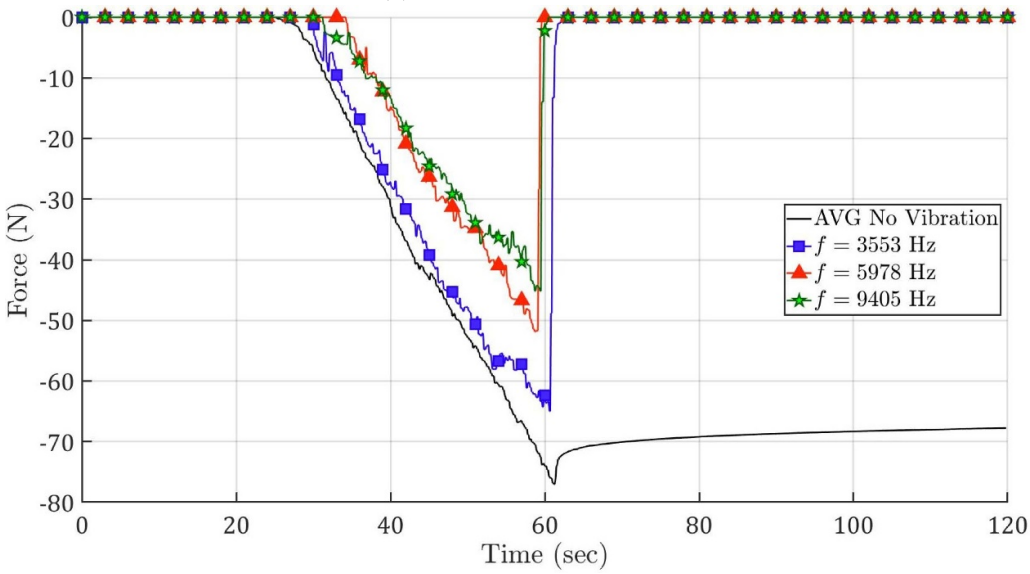

(b) Whirling probe motion

Figure 16. Penetration force with bi-directional modes of vibration.

Table 4. Penetration forces in bi-directional excitation.

Probe motion	f_1 (Hz)	f_2 (Hz)	F^{a}_{max} (N)	R^{b}(%)	$t_r{}^{c}$(s)
No vibration	0	0	77	—	—
Whirling	3553	3553	65	15%	1.5
Whirling	5978	5978	52	32%	0.7
Whirling	9405	9405	45	42%	1.0
Chaotic	3553	5978	51	33%	0.8
Chaotic	9405	5978	50	35%	0.8
Chaotic	3553	9405	45	42%	2.0

[a] Maximum penetration force in Newton.
[b] Percentage of maximum force reduction.
[c] Release time in seconds.

and the other is either 9405 Hz or 3553 Hz. In contrast, the release times were longer when excitations were applied in one direction (uni-direction Bending Vibration), specifically 1.4 s, 2.3 s, and 4.4 s when the voltage was 5978 Hz, 3553 Hz, and 9405 Hz, respectively.

4. Conclusions

We developed a vibro probe to investigate how bending vibrations impact the penetration force into granular materials. This probe exploits bending resonance modes instead of the usual longitudinal vibrations and introduces a new method to improve penetration into granular materials. The probe was equipped with four piezo-electric patches to generate bending vibrations, and we identified its resonance modes through modal analysis. Subsequently, we performed preliminary penetration tests to identify the most effective bending vibration resonance modes for soil fluidization. Then, we conducted main penetration tests to observe the impact of the identified efficient vibration resonances on penetration force. The key findings are as follows:

- **Initial penetration tests:**
  It was noted that for the efficient transfer of vibration energy to soil particles and facilitation of penetration, both displacement and acceleration of vibration of the probe tip are crucial. Resonance frequencies below 3000 Hz and above 10 000 Hz were found to be ineffective due to low acceleration and displacement vibration amplitudes, respectively. In contrast, resonance modes within the 3000–10 000 Hz range exhibited effectiveness, as these frequencies fall within a range where both acceleration and displacement vibration amplitudes are comparatively high compared to the entire frequency spectrum.
- **Main penetration tests (Unidirectional bending vibrations):**
  In the main penetration tests involving unidirectional bending vibrations, frequencies of 5978 Hz and 9405 Hz led to significant reductions in the maximum penetration force by 28% and 21%, respectively. Furthermore, at the end of the penetration process, penetration forces reached zero within 1.4 s and 4.4 sfor the resonance modes of 5978 Hz and 9405 Hz, respectively. During this release period, the deflected shape of the frame returned to its original state by pushing the probe slightly into the fluidized soil sample, and the force in the force sensor reached zero. This indicated that the combined weight of the probe and the linear actuator was sufficient for the slight penetration and instant release of stresses in the structure in the presence of the bending vibrations. Conversely, for the non-vibrating probe, the force sensor only exhibited a 12% reduction in peak force over approximately 59 s. This happened because the deflected structure pushed the probe into the soil to release stresses. However, without bending vibrations, this force was not enough to penetrate the probe slightly into the soil and instantly release stresses in the structure. At a frequency of 3553 Hz, the reduction in the maximum penetration force was less pronounced, but the release time was 2.3 s.
- **Main penetration tests (Bidirectional bending excitation):**
  Bidirectional bending vibrations led to chaotic vibrations when the frequencies differed or whirling motion when they were at the same frequency with a 90-degree phase difference. Significantly, bidirectional excitation demonstrated superior improvements in reducing penetration force compared to unidirectional excitation, as the vibration fluidized the soil in two perpendicular directions. For example, employing a whirling motion with a vibration mode at 9405 Hz in two directions with a 90-degree phase difference resulted in a 42% decrease in the maximum penetration force compared to a non-vibrating probe, and the release time was reduced to 1 s. In terms of release time, the whirling motion at a frequency of 5978 Hz exhibited the fastest duration of 0.7 s, with a 32% reduction in the maximum penetration force.

In summary, our results highlight the potential of unidirectional and bidirectional bending vibrations to reduce the required penetration force and, therefore, can offer a promising solution in the reduction of the size of soil drilling equipment for remote areas.

Data availability statement

All data that support the findings of this study are included within the article (and any supplementary files).

Acknowledgments

This research was undertaken thanks to funding support from the Mitacs E-Accelerate program and the Research Manitoba Innovation Proof-Of-Concept Grant.

Author statement

The authors have the patent ‘Vibratory burrowing probe for investigating subsurface regions of granular media in 1 g and low/microgravity conditions’, pending to Pooneh Maghoul, Mahdi Alaei Varnosfaderani, and Nan Wu (University of Manitoba and PolyValor, with the U.S. Provisional Application No. US Provisional Patent No: 63332775.

Conflict of interest

The authors declare that they have no known competing financial interests or personal relationships that could have appeared to influence the work reported in this paper.

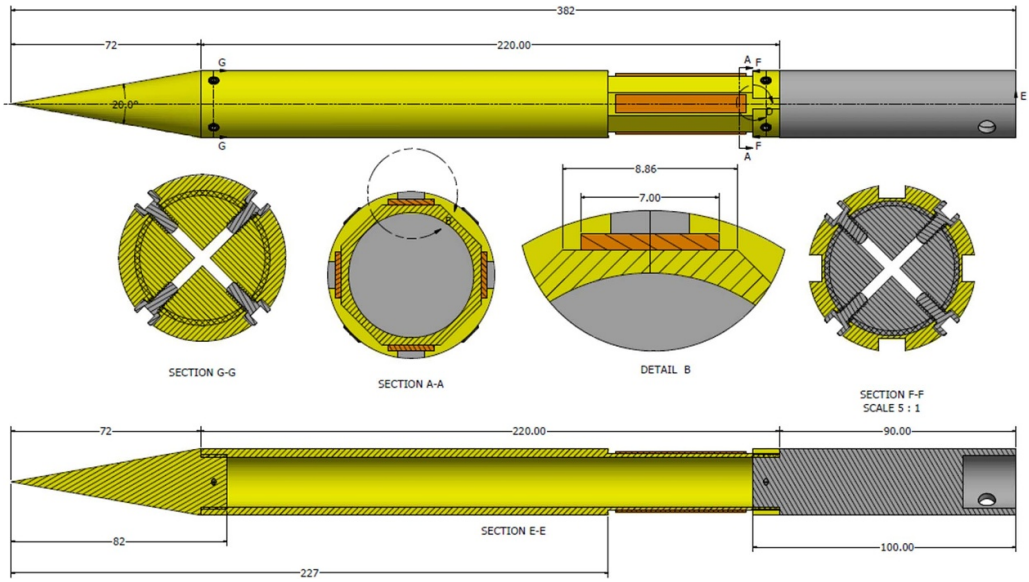

Figure 17. Probe detail drawing (all dimensions are in mm).

Appendix

Figure 17 shows the detail drawing of circular probe-coupling-actuators configuration.

ORCID iDs

Nan Wu https://orcid.org/0000-0001-8768-1328
Pooneh Maghoul https://orcid.org/0000-0003-0457-3968

References

Alaei Varnosfaderani M, Maghoul P and Wu N 2022 Penetration analysis of high-frequency vibro-based probes in granular media using the discrete element method *Earth and Space 2022* (*Denver, Colorado, USA, 25–28 April 2022*) pp 176–83

APC International, Ltd 2021 Physical and piezoelectric properties of APC materials (available at: www.americanpiezo.com/apc-materials/physical-piezoelectric-properties.html) (Accessed 1 September 2023)

Bar-Cohen Y *et al* 2001 Ultrasonic/sonic driller/corer (USDC) as a sampler for planetary exploration *2001 IEEE Aerospace Conf. Proc. (Cat. No. 01TH8542)* (*Big Sky, MT, USA*) vol 1 (IEEE) pp 1/263–1/271

Baumgartner W, Fidler F, Weth A, Habbecke M, Jakob P, Butenweg C and Böhme W 2008 Investigating the locomotion of the sandfish in desert sand using nmr-imaging *PLoS One* **3** e3309

Bolton M D, Gui M W, Garnier J, Corte J F, Bagge G, Laue J and Renzi R 1999 Centrifuge cone penetration tests in sand *Géotechnique* **49** 543–52

Cardoni A, Harkness P and Lucas M 2010 Ultrasonic rock sampling using longitudinal-torsional vibrations *Phys. Proc.* **3** 125–34

Dimitriadis E, Fuller C and Rogers C 1991 Piezoelectric actuators for distributed vibration excitation of thin plates *ASME. J. Vib. Acoust.* **113** 100–7

Dosch J J, Inman D J and Garcia E 1992 A self-sensing piezoelectric actuator for collocated control *J. Intell. Mater. Syst. Struct.* **3** 166–85

Firstbrook D, Harkness P and Gao Y 2014 A novel study on high-powered ultrasonic penetrators in granular material *AIAA SPACE 2014 Conf. and Exposition* p 4265

Firstbrook D, Worrall K, Harkness P, Flessa T, McGookin E and Thomson D 2018a Ultrasonic auger for narrow-gauge borehole drilling *2018 IEEE Int. Ultrasonics Symp. (IUS)* (IEEE) pp 1–4

Firstbrook D, Worrall K, Timoney R and Harkness P 2018b Ultrasonically assisted hammer-action penetrators in planetary regolith *Earth and Space 2018: Engineering for Extreme Environments* (American Society of Civil Engineers Reston) pp 359–68

Firstbrook D, Worrall K, Timoney R, Su nol F, Gao Y and Harkness P 2017 An experimental study of ultrasonic vibration and the penetration of granular material *Proc. R. Soc.* A **473** 20160673

Gao Y, Ellery A, Jaddou M, Vincent J and Eckersley S 2007 Planetary micro-penetrator concept study with biomimetric drill and sampler design *IEEE Trans. Aerosp. Electron. Syst.* **43** 875–85

Omori H, Murakami T, Nagai H, Nakamura T and Kubota T 2012 Development of a novel bio-inspired planetary subsurface explorer: initial experimental study by prototype excavator with propulsion and excavation units *IEEE/ASME Trans. Mechatronics* **18** 459–70

Pitcher C, Alkalla M, Pang X and Gao Y 2020 Development of the third generation of the dual-reciprocating drill *Biomimetics* **5** 38

Sherbrooke W C and Nagle R B 1996 Phrynosoma intraepidermal receptor: a dorsal intraepidermal mechanoreceptor in horned lizards (phrynosoma; phrynosomatidae; reptilia) *J. Morphol.* **228** 145–54

Sherrit S, Bao X, Chang Z, Dolgin B, Bar-Cohen Y, Pal D, Kroh J and Peterson T 2000 Modeling of the ultrasonic/sonic driller/corer: USDC *2000 IEEE Ultrasonics Symp. Proc. An Int. Symp. (Cat. No. 00CH37121)* (IEEE) pp 691–4

Wang Y, Quan Q, Yu H, Bai D, Li H and Deng Z 2018 Rotary-percussive ultrasonic drill: an effective subsurface penetrating tool for minor planet exploration *IEEE Access* **6** 37796–806